JOURNAL OF MATERIALS SCIENCE 22 (1987) 3631–3641

Microstructural development in non-oriented lamination steels

Part 1 The nature of ferrite/pearlite aggregates in continuously cooled low-carbon steels

J.-W. LEE*, P. R. HOWELL
Department of Materials Science and Engineering, The Pennsylvania State University, Pennsylvania 16802, USA

The microstructures produced during continuous cooling of two particular non-oriented lamination steels have been examined using light microscopy, scanning electron microscopy and transmission electron microscopy. In addition to proeutectoid ferrite and pearlite, cementite was present on ferrite grain boundaries and on proeutectoid ferrite/pearlite interfaces. Mechanisms for the formation of these cementite films are presented. The microstructural results demonstrate that ferrite is the "active nucleus" for pearlite in these low-carbon steels. In addition, the data suggest that in addition to branching, the pearlite reaction can be initiated by the nucleation of a series of cementite precipitates on the proeutectoid ferrite/austenite interface.

1. Introduction

1.1. Overview

Generally, a significant amount of electrical energy is lost when electrical steels are used in electromagnetic devices, This loss in energy requires that additional fuel be consumed. Also, additional equipment is necessary to supply this lost energy. The metallurgical industry is therefore paying increasing attention, both to the improvement in quality of existing electrical steels, and to finding new technology which will provide better quality electrical steels. However, it is well known that textural development and other magnetic properties are closely associated with microstructural changes which accompany processing. Therefore, the objective of this overall investigation is to examine microstructural development at each cycle of the processing schedule.

In decarburization, the texture can be obtained by primary recrystallization, but is weak at this stage. Hence, microstructural changes which occur during decarburization are important in obtaining an optimum texture. Decarburization cycles often occur, at least initially, in the two-phase (austenite plus ferrite) region. The kinetics and mechanisms of the ferrite + cementite to austenite transformation are of considerable technological, as well as academic, interest because the austenite so formed, subsequently transforms to ferrite. Similarly, the formation of austenite from ferrite/cementite aggregates is of importance in that dual-phase steels are produced by annealing low-carbon steels in the two-phase (austenite plus ferrite) region, followed by accelerated cooling to transform the austenite to martensite. Therefore, it is necessary to obtain basic information concerning the mechanisms of austenite formation in the intercritical temperature range. However, it would be expected that the reaustenitization characteristics are sensitive functions of the details of the starting structure.

In view of the above, this series of papers is concerned with a microstructural study of one particular class of electrical steels, namely non-oriented lamination steels. It is considered that this investigation is timely in that microstructural development in these steels has received comparatively little attention.

Conventionally, non-oriented lamination steels are processed from hot-rolled strip. Processing involves cold rolling followed by continuous or batch annealing. Finally, the strip is temper rolled and decarburized. Fig. 1 shows the process flow sheet for the lamination steels which have been employed in the present investigation.

Because the microstructures (and indeed, textures) of the final product are influenced by each step in the processing schedule, the first part of the present investigation is concerned with the microstructures developed in the hot-rolled strip. In view of the complex nature of these microstructures, a number of isothermal transformation studies have been performed and analysed (Part 2 of this series of papers).

The effect of cold-rolling, followed by continuous annealing and temper rolling, on the nature of the experimental materials is documented in Part 3. Part 4 investigates the effects of cold rolling alone and cold rolling plus annealing on the microstructures of the as-received hot-rolled strip.

Decarburization involves both the formation of austenite and its subsequent dissolution. The reaustenitization behaviour (in the absence of a decarburizing

Present address: Department of Metallurgical Engineering and Materials Science, Carnegie-Mellon University, Pennsylvania 15213, USA.

0022–2461/87 $03.00 + .12 © *1987 Chapman and Hall Ltd.*

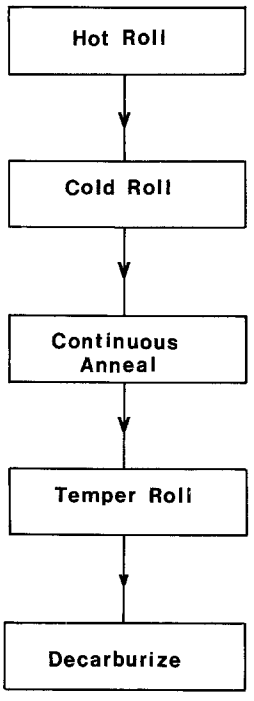

Figure 1 Process flow diagram.

atmosphere) of the lamination steels is discussed in Part 5. Part 6 presents the results of a preliminary investigation concerning decarburization of the temper-rolled material.

1.2. Background

Previous investigations of electrical lamination steels have been concerned primarily with the development of texture and the control of grain size in order to reduce magnetic losses. Because it is well known that carbon has a major effect on these losses, it is of scientific and practical importance to correlate carbide distributions with microstructural changes during each cycle of the processing schedule. Therefore, as a part of the overall investigation concerning the microstructural development in cold-rolled lamination steels, the nature of the ferrite/pearlite aggregates in the starting material, i.e. continuously cooled low-carbon steels, has been examined. In addition, the effect of cooling rate has been simulated by reaustenitizing the starting material followed by either air or furnace cooling.

When hypoeutectoid steels are slowly cooled from the single-phase austenite region to room temperature, the product constituents are ferrite, pearlite and cementite. The nature of the nucleation and growth of pearlite has been studied extensively by Mehl and his colleagues [1, 2] and was reviewed in the 1962 Proceedings of the conference on the "Decomposition of Austenite by Diffusional Process" [3]. However, some questions still remain concerning the proposed mechanisms for nucleation and growth. For example, Hull and Mehl [1] suggested that cementite is the active nucleus and that a pearlite colony forms by simultaneous edgewise and sidewise growth through the repeated nucleation of ferrite and cementite. Their version of the nucleation and growth of pearlite has been criticized by several investigators [4–6]. Hillert [4] argued that no sideways growth occurs, but that the number of lamellae is increased by branching from a single stem of cementite. It is believed [5, 6] that either ferrite or cementite can be the active nucleus for pearlite (i.e. the only nucleation event which is required to form a pearlite colony is that of ferrite or cementite on the proeutectoid phase/austenite interface) depending on the carbon content. However, it has also been suggested [7, 8] that pearlite can form by either mechanism, i.e. by branching and by repeated sideways nucleation.

During the decomposition of austenite in continuously cooled low-carbon steels, much of the carbon is used to form pearlite. However, carbon is also retained in the ferrite and precipitates out slowly with time. Cementite films at ferrite grain boundaries have been observed by several investigators and two different mechanisms of the formation of the films have been proposed [9–20]: direct transformation from austenite films and precipitation of carbon from supersaturated ferrite. However, it is still not clear why pearlite colonies are often surrounded by an almost continuous film of cementite and why massive films of cementite are located on the ferrite grain boundaries.

In the context of the above, the objectives of the present investigation are (1) to examine the overall distribution of the microconstituents in continuously cooled low-carbon steels; (2) to analyse the formation of films of cementite; (3) to determine the effect of cooling rate on the formation of cementite films; and (4) to investigate the formation of pearlite in hypoeutectoid steels.

2. Experimental details

Two particular low-carbon hot-rolled steel strips (2.5 mm thick) were obtained from Inland Steel, Chicago, Illinois, and the chemical compositions are given in Table I. To study the effect of cooling rate on the nature of the pearlite/ferrite aggregates, specimens were austenitized at 1000° C for 5 min. The austenitized materials were either furnace cooled or air cooled.

Specimens for light and scanning electron microscopy (SEM) were prepared using standard metallographic techniques and etched in 2% nital. SEM examinations were conducted on an I.S.I. Super IIIA operating at 25 kV. Specimens for transmission electron microscopy (TEM) were prepared in a twin-jet electropolisher using an electrolyte consisting of 5% perchloric acid in glacial acetic acid at room temperature and at a potential of 35 V. TEM was performed using a Philips EM 300 operating at 100 kV. Volume fraction and size measurements were obtained using standard stereological techniques.

3. Results

3.1. Microstructures of the as-received steels

Figs 2a and b are typical light micrographs of steels A and B, respectively. The ferrite is predominantly

TABLE I Chemical compositions (wt %) of specimen materials

	C	Mn	Si	P	S	Al
Steel A	0.04	0.6	0.05	0.06	0.02	< 0.008
Steel B	0.04	0.7	0.22	0.09	0.02	0.21

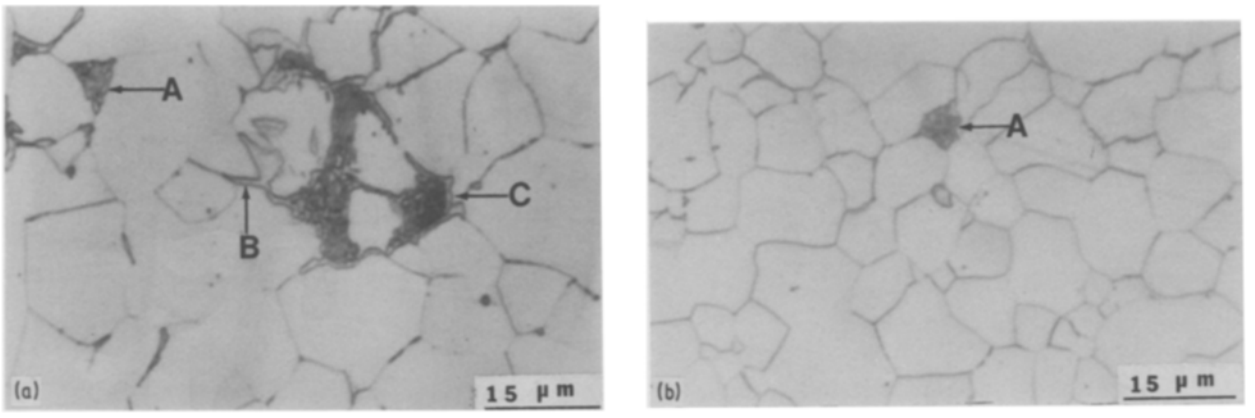

Figure 2 Light micrographs of the as-received hot-rolled steels. (a) Steel A, (b) Steel B.

equiaxed and isolated islands of pearlite (arrowed A in the figures) are observed. Grain-boundary precipitation of cementite is also extensive (arrowed B in Fig. 2a) and the pearlite colonies are often surrounded by an almost continuous film of cementite (arrowed C in Fig. 2a). The observation of cementite films was more frequent in steel A than in steel B. For both steels, the volume fraction of pearlite was found to be $\sim 3.5\%$, while the ferrite grain sizes were 35 and 27 μm for steels A and B, respectively.

Two types of cementite precipitate were observed at ferrite grain boundaries; the first is a "massive film" whilst the other is discrete in nature. Figs 3 and 4 illustrate both types of cementite precipitate. In the former figure (from steel A), almost continuous massive films of cementite are shown whilst discrete precipitates of cementite are illustrated in Fig. 4 (from steel B). The discrete precipitates assumed a plate-like morphology and frequently led to puckering of the ferrite boundaries (Fig. 4). In addition, these precipitates tended to be much thinner than the films of cementite (compare Fig. 4 with Fig. 3).

Figs 5 and 6 are SEM images of pearlite colonies from steels A and B, respectively. In both instances, the cementite within the pearlite is approximately lamellar. In common with the light microscopy results, the proeutectoid ferrite/pearlite interfaces are seen to be associated with coarsened cementite. In Fig. 5, massive films of cementite are observed at the proeutectoid ferrite/pearlite interface (A) and at the adjacent ferrite grain boundary (B). It is also interesting to note that films A and B are apparently continuous. In contrast, little evidence for completely continuous films of cementite in Steel B was observed, either at proeutectoid ferrite/pearlite interfaces or at ferrite grain boundaries (see Fig. 6). It should be noted that not all proeutectoid ferrite/pearlite interfaces are associated with coarsened cementite as shown in Fig. 5. For this latter interfacial type, no boundary is apparent between the proeutectoid ferrite grain (in this instance grain 1 in Fig. 5) and the pearlitic ferrite. This observation suggests that the proeutectoid ferrite is the active nucleus (as defined in Section 1.2) for the formation of pearlite, because the pearlitic ferrite is continuous with the proeutectoid ferrite. Evidence for the initiation of continuous film formation by a coarsening process is seen at the impingement interfaces between pearlite and proeutectoid ferrite in Fig. 6 and the "tips" of the cementite lamellae exhibit a "club-like" morphology at the impingement interfaces (arrowed A in Fig. 6). It should be noted that the grain-boundary films of cementite in steel B (arrowed B on Fig. 6) are generally thinner and less prevalent than in steel A.

Figs 7 and 8 are bright-field transmission electron micrographs of steels A and B, respectively. In both materials a relatively low free-dislocation density was observed, and the majority of the dislocations had formed sub-boundaries. The observation of sub-boundaries is consistent with other studies on slowly cooled low-carbon steels [21]. Sub-boundary formation can be explained by polygonization of dislocations,

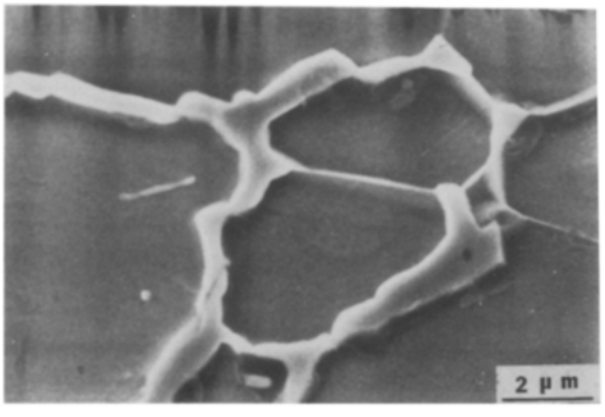

Figure 3 Massive films of cementite at ferrite grain boundaries (steel A).

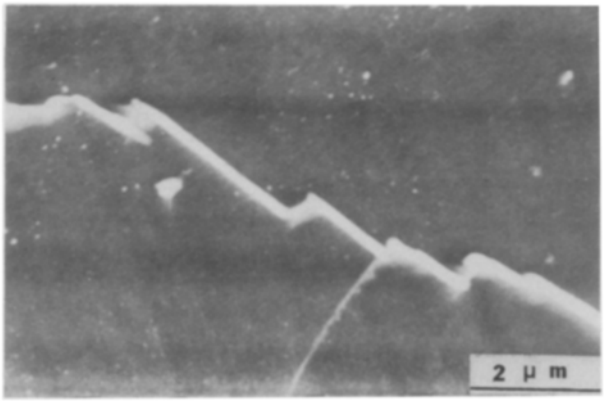

Figure 4 Discrete precipitates of cementite at ferrite grain boundaries (steel B). Note the pronounced puckering of the boundary.

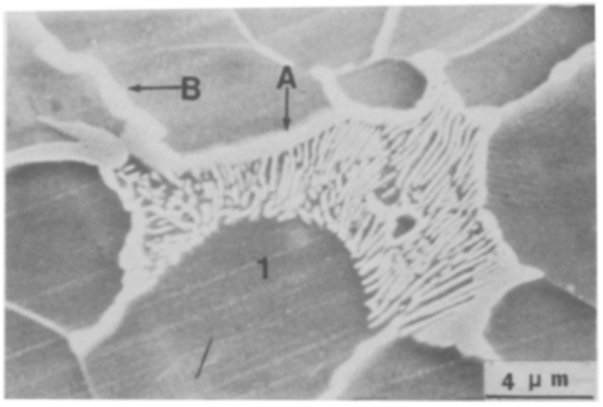

Figure 5 SEM image of a pearlite colony in Steel A showing massive films of cementite, both at ferrite grain boundaries (B), and at pearlite/proeutectoid ferrite interfaces (A).

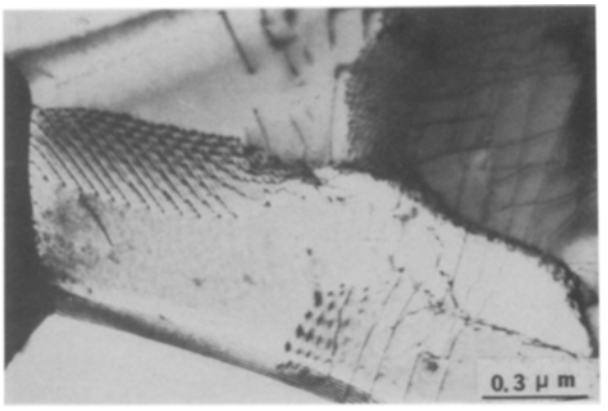

Figure 7 A bright-field micrograph of sub-boundaries in proeutectoid ferrite (steel A).

the latter being created during the transformation and by the transformation strains.

Figs 9 and 10 show examples of the nature of discrete cementite precipitates in steel B. The cementite plates were often at a low angle to the grain boundary which led to puckering of the boundaries (see Figs 9 and 10). In addition, precipitation of cementite occurred at ferrite triple junctions (arrowed A in Fig. 9).

The distribution of cementite in Fig 11 is somewhat unusual and two possible explanations can be advanced: (1) they are discrete precipitates of cementite which have led to extensive puckering of the ferrite grain boundary; and (2) this is an "embryonic" pearlite colony which formed from a small pool of austenite, ferrite grain A being the active nucleus.

Fig. 12a is a typical bright-field micrograph of a massive cementite film at a ferrite grain boundary, whilst Fig. 12b is a cementite centred dark-field image corresponding to Fig. 12a. The cementite film is not continuous as might be inferred from the light micrographs and SEMs of Figs 2 and 5. Instead, it is composed of multiple precipitates of cementite which have impinged. It should also be noted that the individual cementite precipitates have different orientations as is shown in the centred dark-field image of Fig. 12b and the observation of cementite grain boundaries in Fig. 12a.

Fig. 13a is a bright-field micrograph of an "interface" between a pearlite colony and proeutectoid ferrite, whilst Fig. 13b is the corresponding ferrite dark-field image. It can be seen that no grain boundary is present between proeutectoid ferrite grain 1 and the pearlitic ferrite, and thereby, the proeutectoid ferrite has the same orientation as the pearlitic ferrite. This lends further support to the contention that proeutectoid ferrite is the active nucleus for the formation of pearlite in hypo-eutectoid steels.

Transmission electron micrographs of pearlitic colonies and associated impingement interfaces are shown in Figs 14 and 15. In Fig. 14, the pearlite/proeutectoid ferrite interface is covered with a massive film of cementite (arrowed). In common with Fig. 12, the film is composed of several cementite precipitates which have coalesced. It is suggested that this film is not created by the impingement of cementite lamellae within the pearlite colony, with the proeutectoid ferrite, in that the film is not in contact with the cementite lamellae. Rather, it appears that nucleation of this film occurs independently of any impingement event and is associated with the nucleation and growth of cementite on the proeutectoid ferrite grain 1/austenite interface prior to impingement with the pearlitic colony (see Section 4.2). In Fig. 15 (from steel B), the cementite lamellae exhibit a "club-like" morphology in the vicinity of the impingement interface (see also Fig. 6) and have coarsened at this interface. It is suggested that continued coarsening at the interface will lead eventually, to a "massive" film of cementite.

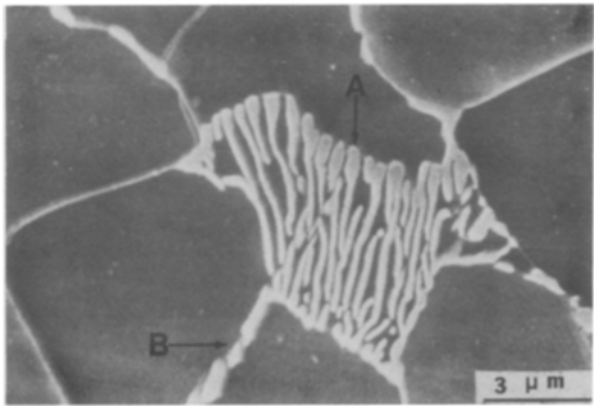

Figure 6 A pearlite colony in steel B. The pearlite lamellae in the vicinity of the impingement interface (A) have assumed a "club-like" morphology.

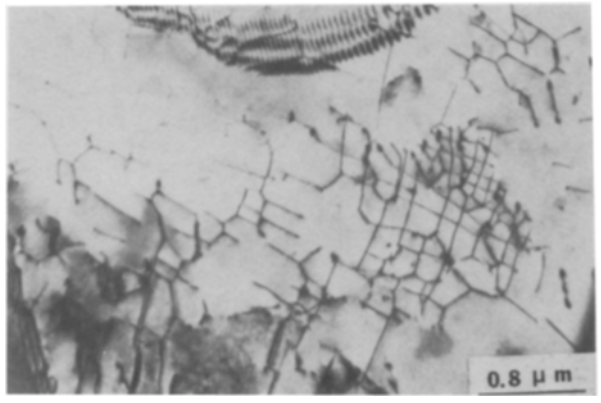

Figure 8 Ill-formed sub-boundaries in proeutectoid ferrite (steel B).

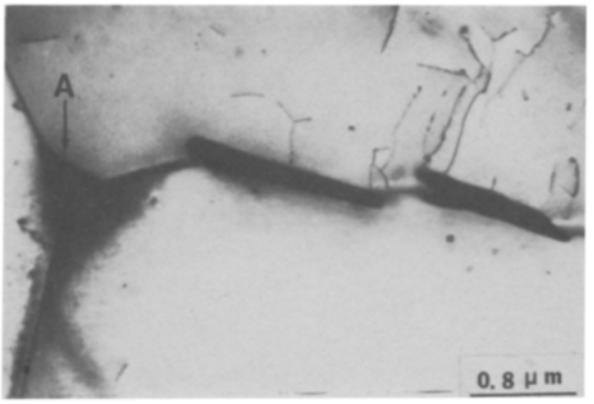

Figure 9 Discrete cementite precipitates, both at ferrite grain boundaries and at the triple junction (A) (steel B).

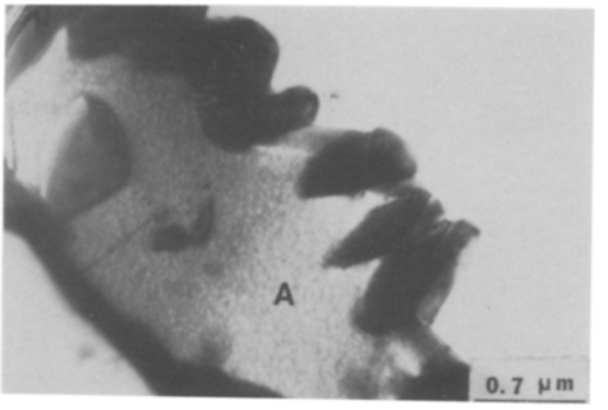

Figure 11 An array of grain-boundary cementite precipitates in steel B (for discussion: see text).

3.2. The microstructures developed in air-cooled and furnace-cooled steels

The results presented in the previous section showed that there were significant differences between steels A and B. These differences could be attributed to differences in coiling temperature, cooling rate or alloy chemistry. However, the as-received steels had been processed commercially and no conclusion can be made concerning the origin of the differences observed. In an attempt to examine the effect of cooling rate, the steels were re-austenitized and either air or furnace cooled.

Figs 16 and 17 are light micrographs of furnace-cooled and air-cooled steels, respectively. In the furnace-cooled steels (Fig. 16) massive cementite films are extensive at ferrite grain boundaries (arrowed A in Figs. 16a and b) and at the proeutectoid ferrite/pearlite interfaces (arrowed B in Figs 16 a and b). For the air-cooled specimens, cementite precipitates are still observed at the grain boundaries (arrowed C in Figs. 17a and b). However, cementite films at proeutectoid ferrite/pearlite interfaces are apparently absent in the air-cooled steels and pearlite colonies with high aspect ratios are often observed (arrowed D in Figs. 17a and b). Comparison of furnace-cooled steel A with furnace-cooled steel B also indicates that the formation of massive films at the pearlite/ferrite and ferrite/ferrite interfaces is more prevalent in steel A than in steel B as was observed in the as-recieved steels. This is most likely a reflection of the differences in alloy chemistry between steels A and B (Table I).

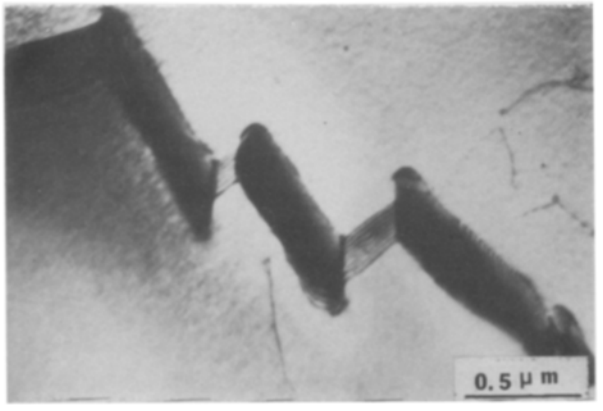

Figure 10 Grain-boundary precipitation of cementite which has led to puckering of the ferrite grain boundary (steel B).

The overall effect on pearlite morphologies by changing cooling rate is complex. Figs. 18–21 are SEMs of pearlite colonies both from furnace-cooled steel A (Figs 18, 19) and from air-cooled steel A (Figs 20, 21). Irregular cementite lamellae developed upon air cooling (e.g. Fig. 21), whereas for furnace cooling, the cementite in the pearlite colonies remains approximately lamellar (Fig. 18). Coarsening of cementite at proeutectoid ferrite/pearlite interfaces is observed irrespective of cooling rate, although the films are more extensive in furnace-cooled specimen materials. In common with the as-received materials, certain interfaces are not associated with coarsened cementite. In Fig. 18, continuity between proeutectoid ferrite grain 1 and the pearlitic ferrite is observed. In addition, there are apparently two types of massive cementite film (A and B in Fig. 18). Film type A is the same as that shown in Fig. 5. However, film type B seems to be considerably wider and appears to have encapsulated regions of ferrite (arrowed C). The reason for the type B film is uncertain. However, it is possible that the impingement interfaces (B) are at a shallow angle to the plane of polish so that the large apparent width of these films is simply a sectioning effect. The islands of ferrite within these films could then be explained by the incomplete coverage of the impingement interface by cementite. In Fig. 19, massive films of cementite are extensive at ferrite grain boundaries, and the small pearlite colonies (A and B) are completely covered with a film of cementite. In addition, the films associated with the small pearlite colonies are continuous with the grain-boundary cementite films. It might be inferred from Fig. 19 that the continuous films at the ferrite boundaries, at the ferrite/pearlite interfaces, together with the pearlite colonies themselves, are formed directly during the decomposition of austenite. Similarly, it can be suggested that the films which envelop the pearlite colonies can form by the same mechanism as that which produces the films at ferrite grain boundaries (see Section 4.2).

In the air-cooled specimens, bands of pearlite are a frequent occurrence (arrowed in Fig. 20) and individual colonies comprise irregularly spaced and

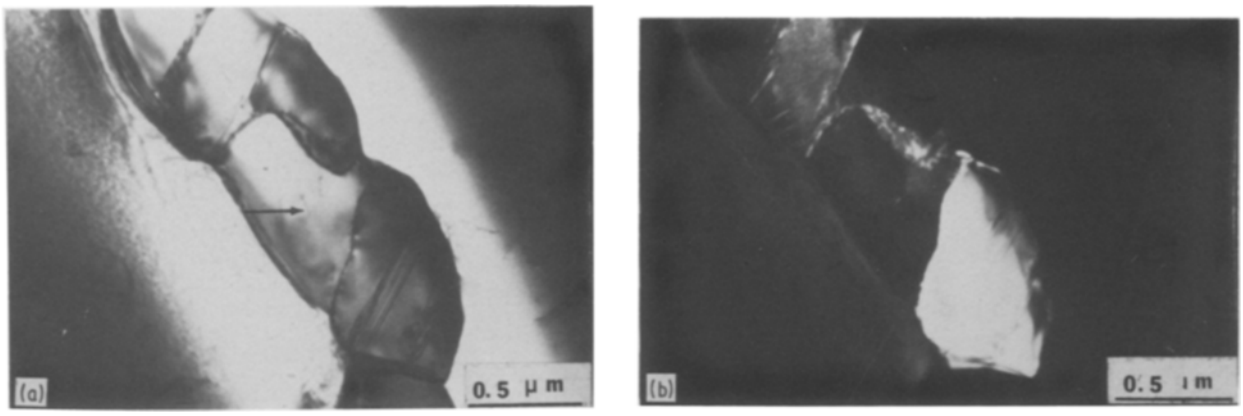

Figure 12 TEM of a massive cementite film at a ferrite grain boundary (steel A). (a) Bright-field image, (b) a corresponding cementite centred dark-field image.

oriented cementite lamellae (see Figs. 20, 21). Furthermore, some areas in the pearlite colonies are devoid of cementite lamellae, e.g. at A in Fig. 21 (and see Fig. 17a). It should be noted that these observations were made only in air-cooled steels and not in as-received and furnace-cooled steels.

The pearlite colony A in Fig. 22 (furnace-cooled steel B) is of interest in that the pearlite is divergent. This, taken together with the observation that there is continuity between the proeutectoid ferrite (grain 1) and the pearlitic ferrite, suggests that this pearlite colony formed by the branching mechanism of Hillert [4]. In contrast, the formation of the pearlite colony in Fig. 23 can be rationalized if this pearlite developed by multiple nucleation of cementite on the austenite/proeutectoid ferrite interface in a manner similar to that described in the conventional mechanism for discontinuous reactions [22] (and see [23]).

In common with the as-received steels, discrete cementite precipitates at ferrite grain boundaries were often observed in both steels irrespective of cooling rate.

In air-cooled steels, a higher number density of pearlite colonies form when compared with the furnace-cooled material. As shown in Fig. 24 (from steel B), the ferrite grain boundaries are associated with thin films of cementite (arrowed A) and needle- or plate-like pearlite colonies are also observed (arrowed B).

4. Discussion

4.1. General discussion

The results detailed in Section 3 can be summarized as follows:

1. Pearlite colonies consist predominantly of well developed lamellar structures in slowly cooled steels, whilst in air-cooled steels, they are comprised of a non-uniform distribution of cementite.
2. Proeutectoid ferrite is often continuous with pearlitic ferrite.
3. Massive cementite films and discrete precipitates of cementite at grain boundaries are a frequent occurrence.
4. Many pearlite/proeutectoid ferrite interfaces are associated with a continuous film of cementite.
5. Massive cementite films, both at grain boundaries and at the interface between pearlite and proeutectoid ferrite consist of many cementite precipitates.
6. The formation of the films at grain boundaries and ferrite/pearlite interfaces is more prevalent in the as-received/furnace-cooled steel A than in the as-received/furnace-cooled steel B.
7. The propensity for the formation of films is more extensive in furnace-cooled steels than in air-cooled steels.
8. Puckering of the grain boundaries accompanies the precipitation of discrete particles of cementite.

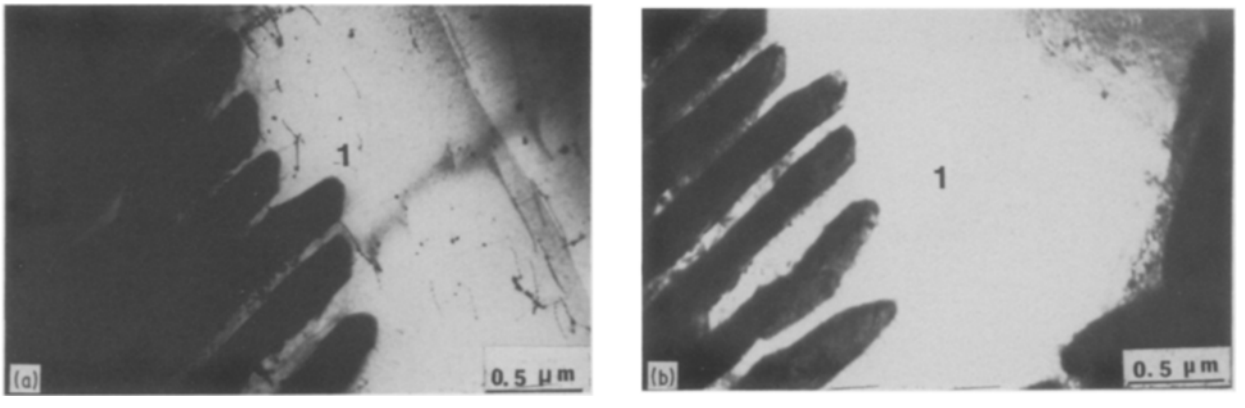

Figure 13 A pearlite colony from steel B showing that the proeutectoid ferrite is continuous with the pearlitic ferrite. (a) Bright-field image, (b) centred dark-field image.

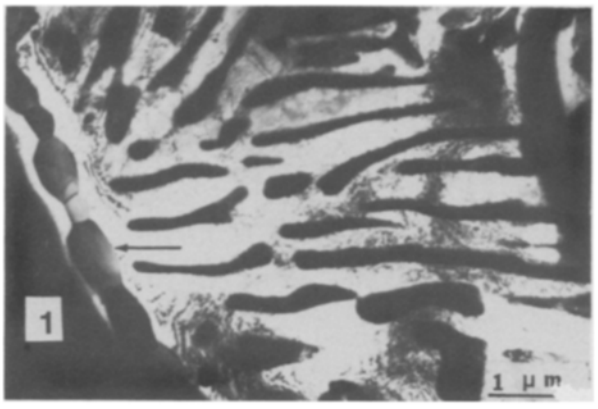

Figure 14 A massive film of cementite at the proeutectoid ferrite/pearlite interface. Note that the interface is not in contact with the cementite lamellae within the pearlite (steel A).

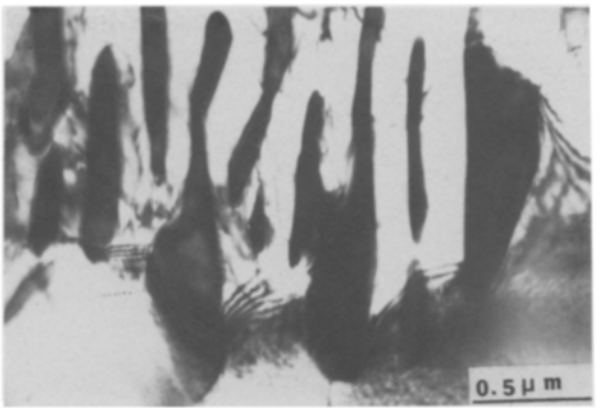

Figure 15 An impingement interface between proeutectoid ferrite and pearlite (steel B).

The lamellar structure of the pearlite is not unexpected in the as-received and furnace-cooled steels because of slow cooling through the transformation temperature. The irregularity of the pearlitic cementite in the air-cooled steels is somewhat harder to rationalize. However, the temperature at which the pearlite reaction is initiated will be lower during air-cooling [24]. Hence, it is likely that the rapid kinetics of the pearlite reaction in the air-cooled samples will lead to irregular pearlitic structures. The effect of cooling rate on the pearlitic reaction is considered in further detail elsewhere [23].

Coarsened cementite at pearlite/ferrite and ferrite/ferrite interfaces can form by direct transformation of austenite, whilst the coarsened cementite at the "tips" of cementite lamellae can develop by the impingement of the cementite lamellae with a pre-existing proeutectoid ferrite grain. An explanation for the formation of the "club-like" morphology will be given in Section 4.2 (and see [23]).

4.2. Formation of massive cementite films at grain boundaries and at pearlite/ferrite interfaces

Samuels [19] suggested that "films of cementite are not present at ferrite grain boundaries for carbon contents greater than 0.3%". His contention is inconsistent with other results where the films were observed in steels containing up to 0.6% carbon [15–18]. Thus, it can be inferred that the formation of cementite films is related both to the cooling rate and alloy chemistry, but not to the carbon content alone. This contention is in agreement with the results presented in Section 3 because (1) the propensity for the formation of massive films of cementite is much more extensive in furnace cooled steels than in air-cooled steels, and (2) the formation of the films is more prevalent in as-received/furnace-cooled steel A than in as-received/furnace-cooled steel B.

Three possibilities for cementite film formation can be proposed in the context of the results presented in Section 3: (1) the massive films at ferrite grain boundaries form directly from austenite with a high aspect ratio; (2) the massive films at pearlite/ferrite interfaces are due to the nucleation and growth of cementite on the proeutectoid ferrite/austenite interfaces prior to impingement with a pearlite colony; and (3) the films develop by a coarsening process at the impingement interface of pearlite with proeutectoid ferrite via diffusion of carbon from supersaturated ferrite. Generally, it has been found [25] that large volumes of of austenite transform to pearlite, but small volume austenite (2 to 4 μm wide) are likely to form massive cementite films directly at ferrite grain boundaries. However, it has been shown that these films are composed of differently oriented multiple precipitates of cementite (see Fig. 12b). Fig. 25 illustrates schematically the development of cementite films at ferrite grain boundaries. The first step (Fig. 25b) is the formation of multiple nuclei of allotriomorphic cementite at one austenite/proeutectoid ferrite interface (it

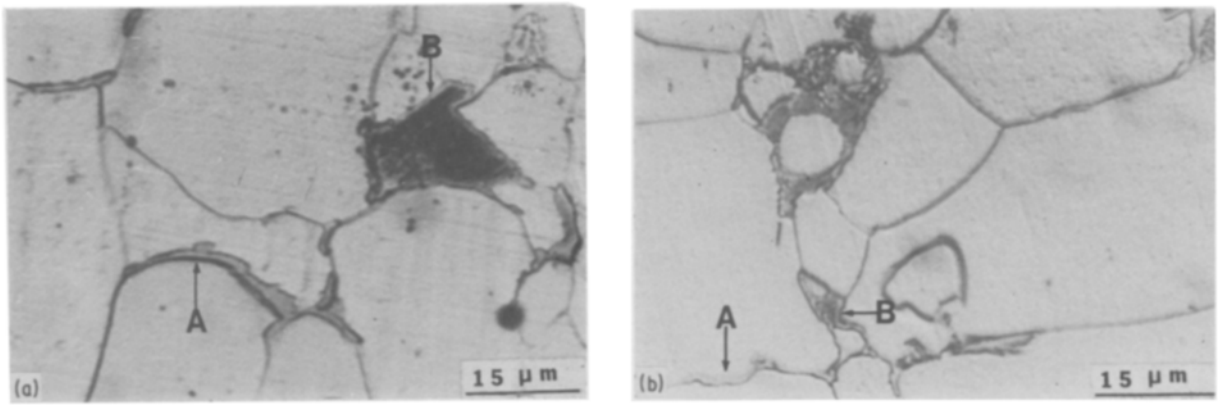

Figure 16 Light micrographs of furnace-cooled steels, (a) steel A, (b) steel B.

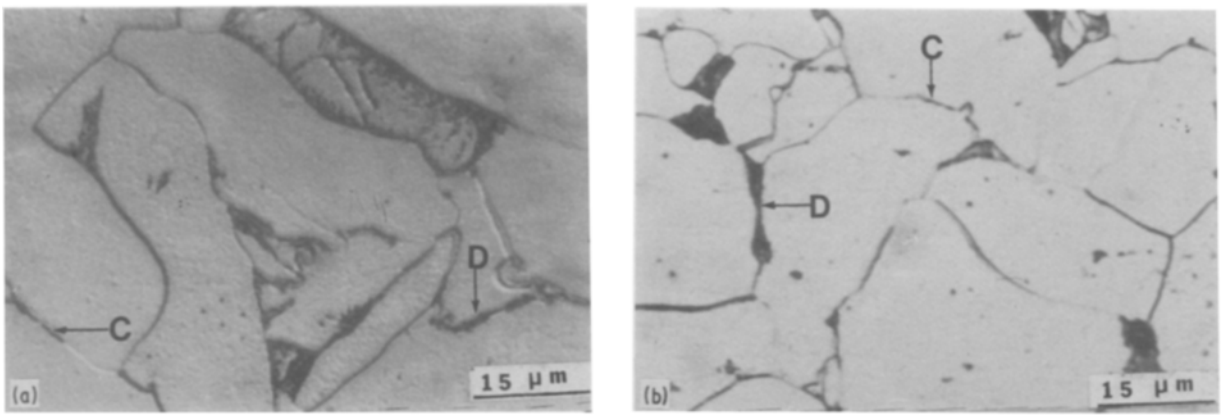

Figure 17 Light micrographs of air-cooled steels, (a) steel A, (b) steel B.

is assumed that the austenite has a high aspect ratio). Subsequent growth can be achieved by diffusion of carbon through the austenite. This diffusion leads to a depletion of carbon and consequently, the growth of ferrite grain 1 (α_1 in Fig. 25c). Finally, the proeutectoid grains α_1 and α_2 will impinge to create the grain-boundary cementite film. It should be noted that this model assumes that precipitation at the α_2/γ interface effectively immobilizes this interface. Further growth of the cementite film can occur during subsequent cooling by carbon diffusion through the supersaturated ferritic matrix.

Massive cementite films at pearlite/proeutectoid ferrite interfaces can form in a manner which is similar to that at ferrite grain boundaries as is shown in Fig. 26. In the first stage, nucleation of the pearlite colony has occurred as has the formation of discrete precipitates on the austenite/proeutectoid ferrite interface (Fig. 26a). In common with film formation at ferrite grain boundaries it is suggested that a number of cementite precipitates develop. Growth is then achieved by volume diffusion of carbon through the remaining austenite and from the supersaturated ferrite. However, as the growing pearlite colony approaches the film, the colony will encounter a carbon-depleted zone. Thus, the growth of the pearlite will cease and the remaining austenite will transform to proeutectoid ferrite as shown in Fig. 26c. This schematic figure is similar to the experimental image of Fig. 14. However, the observation that pearlitic cementite is often in contact with the massive films, suggests that either carbon depletion in austenite occurs to a limited extent only or that this mechanism of film formation occurs infrequently [26].

In addition to the massive films, cementite lamellae at the impingement interfaces often exhibit a "club-like" morphology (see Figs 6 and 15). Fig. 27 is a schematic illustration of a possible mechanism for the development of this morphology. After the impingement of cementite lamellae with proeutectoid ferrite (the latter not being associated with cementite precipitates), the tips of the cementite lamellae can grow by accretion of carbon from supersaturated ferrite during cooling. The final shape of the cementite at the impingement interface will be determined by balancing interfacial tension forces at the triple junctions as shown in Fig. 27c.

From Fig. 27c

$$\gamma_{\alpha\alpha} = \gamma_{\alpha C_p} \cos \phi_1 + \gamma_{\alpha C_l} \cos \phi_2 \qquad (1)$$

where $\gamma_{\alpha\alpha}$ = the $\alpha|\alpha$ grain-boundary energy, $\gamma_{\alpha C_p}$ = the energy of the partially coherent ferrite/cementite interface, $\gamma_{\alpha C_l}$ = the energy of the incoherent ferrite/cementite interface. It appears unlikely that the source of carbon for this reaction is from the cementite within the pearlite colony because the lamellar widths do not appear to decrease in the vicinity of the impingement interface. It should also be noted that the coarsened cementite at the impingement interface could develop into a massive film if sufficient time for coarsening is allowed (see [26]).

The results described in Section 3.2 revealed that the

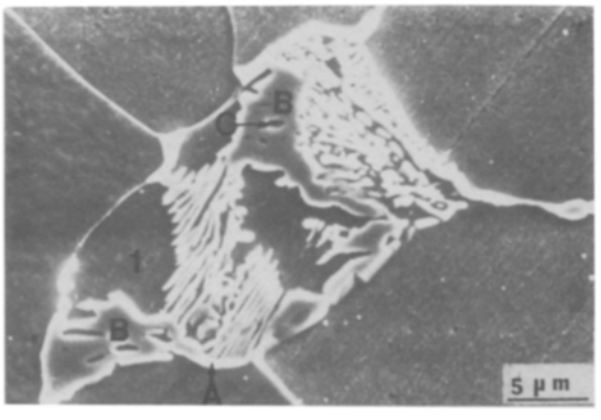

Figure 18 SEM (furnace-cooled steel A) of a pearlite colony which is associated with massive films of cementite.

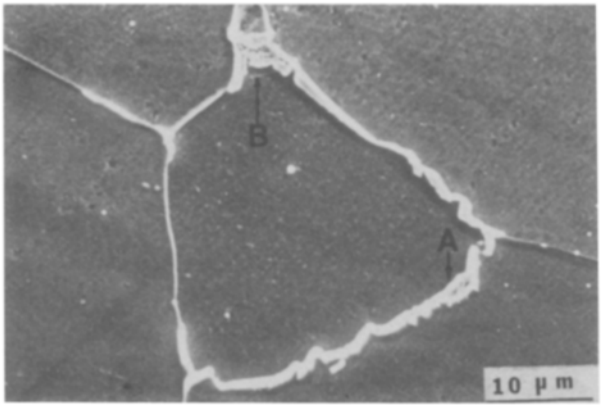

Figure 19 SEM showing massive films of cementite on ferrite grain boundaries (furnace-cooled steel A).

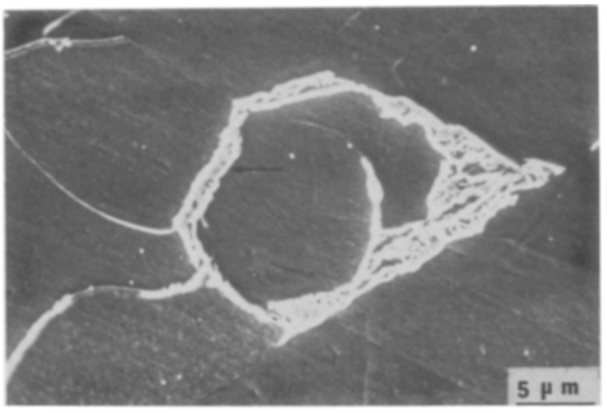

Figure 20 Bands of pearlite colonies showing irregularity oriented cementite lamellae (air-cooled steel A).

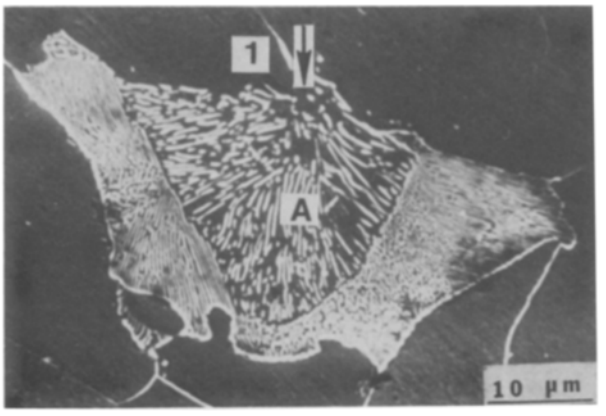

Figure 22 SEM image of a pearlite colony (A) which most probably formed by a branching mechanism (furnace-cooled steel B).

cementite films were thinner in air-cooled steels than in furnace-cooled steels. This can be rationalized as follows. The massive films are formed by two separate processes: (1) direct transformation from austenite; and (2) coarsening after the pearlite reaction due to a residual carbon supersaturation. In the air-cooled steels, because of the faster cooling rate, the overall diffusivity of carbon is slower and thereby the contribution of carbon from supersaturated ferrite, to the coarsening of the cementite film is expected to be less. In addition, the observation of a higher number density of pearlite colonies in the air-cooled steels, suggests that there are more sinks for the residual carbon which will further reduce the coarsening of individual cementite films.

Both the differences in cooling rate and the size of the austenite are important factors in film formation. In addition, in Section 3 it was shown that the formation of a massive film of cementite is more prevalent in as-received/furnace-cooled steels A than in as-received/furnace-cooled steel B. This is evidence that alloy chemistry also plays an important role in the formation of these films. It has been suggested [11, 17, 25] that of the alloying elements, manganese reduces the propensity for the formation of cementite films and its effect has been attributed to changes in the interfacial energies between austenite, ferrite and cementite as a function of manganese content [25]. Reference to Table I shows that the difference in manganese content for steels A and B is only 0.1%. This is unlikely to lead to any marked change in behaviour. Similarly, silicon and aluminium contents should have little effect [27]. However, steel B contains 0.09%P whereas steel A contains 0.06%P. Because phosphorus is a highly surface-active element, it is possible that segregation of the phosphorus can change the relative interfacial energies, thereby reducing the tendency for film formation in steel B. Obviously, more work is required to understand fully the effect of various solute elements on the decomposition of austenite.

4.3. The formation of discrete cementite precipitates

The formation of discrete precipitates of cementite (e.g. Figs 4, 9 and 10) is due most likely to precipitation from supersaturated ferrite during cooling. This supersaturation arises due to the different solubilities of carbon in α-iron from the eutectoid temperature to room temperature. The discrete precipitates also led to extensive grain-boundary puckering. This phenomenon has been documented in a variety of systems which exhibit a discontinuous reaction and is suggested to be because of a reduction in the overall energy barrier to nucleation.

4.4. Nucleation and growth of pearlite

The results of Section 3 are fully consistent with proeutectoid ferrite being the active nucleus for pearlite. Considering the formation of a pearlite colony when the branching mechanism is operative, it has been suggested [4] that the lamellar structure can only

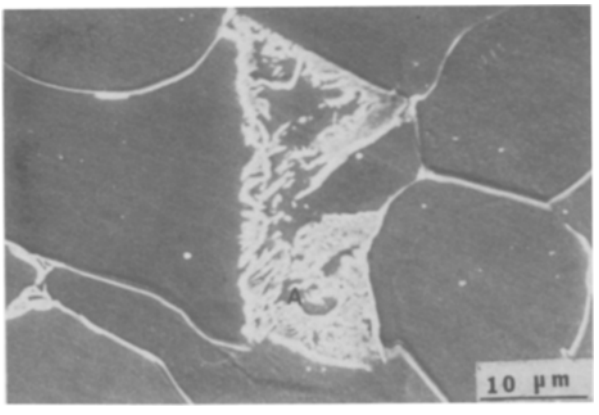

Figure 21 Pearlite colonies exhibiting regions which are devoid of cementite lamellae (A) (air-cooled steel A).

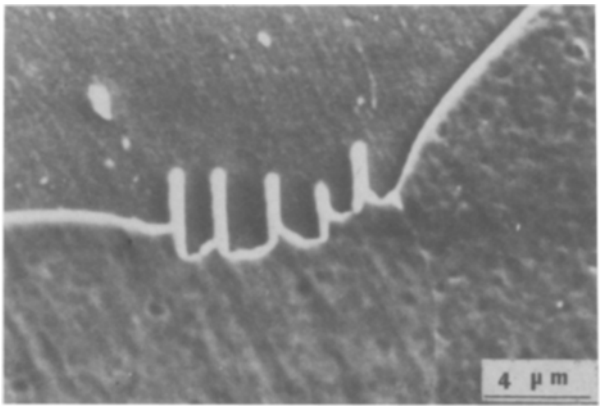

Figure 23 SEM image of a pearlite colony (furnace-cooled steel B).

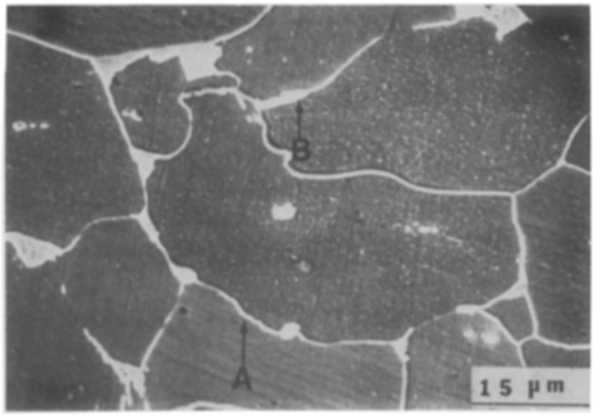

Figure 24 SEM image of pearlite colonies (air-cooled steel B).

be obtained by cooperative growth. The colony shown in Fig. 22 exhibits characteristics that are consistent with the branching model of Hillert [4]. In contrast, Fig. 23 suggests that cooperative growth is established almost immediately and that multiple nucleation of cementite is often the formative step in the initiation of a pearlite colony [23].

As shown in Section 3.2. for the air-cooled steels, some regions in the pearlitic colonies are devoid of cementite lamellae. Reasons for this observation are given in Thompson [23]. Bands of pearlite (Fig. 20) and needle- or plate-like pearlite colonies (Fig. 24) are also a frequent occurrence in air-cooled steels. It would appear that austenite with a high aspect ratio develops into a massive film of cementite in furnace-cooled steels (see Fig. 18), whilst austenite of a similar morphology in the air-cooled steels often transforms to pearlite colonies of a high aspect ratio (see Fig. 20). It would appear that at the lower temperatures associated with pearlite formation in air-cooled steels, the probability of thin austenite films transforming to pearlite is greater than at higher temperatures.

5. Conclusions

1. Pearlite/proeutectoid ferrite interfaces in hot-rolled specimens are often associated with an almost continuous film of cementite.

2. Massive cementite films at ferrite grain boundaries are a frequent occurrence.

3. (a) The formation of cementite films at grain boundaries is due to the direct transformation of austenite of a high aspect ratio. (b) Massive cementite films at proeutectoid ferrite/pearlite interfaces can form by precipitation of cementite on the proeutectoid

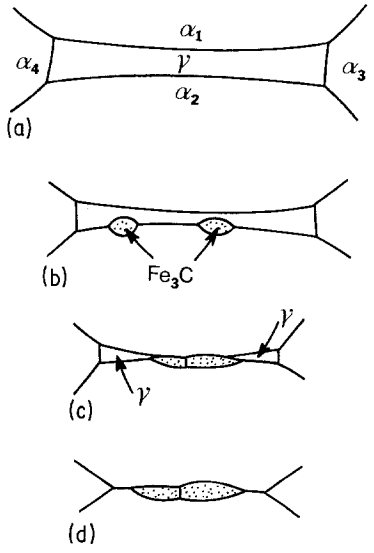

Figure 25 Schematic illustration for the development of massive cementite films at proeutectoid ferrite/austenite interfaces.

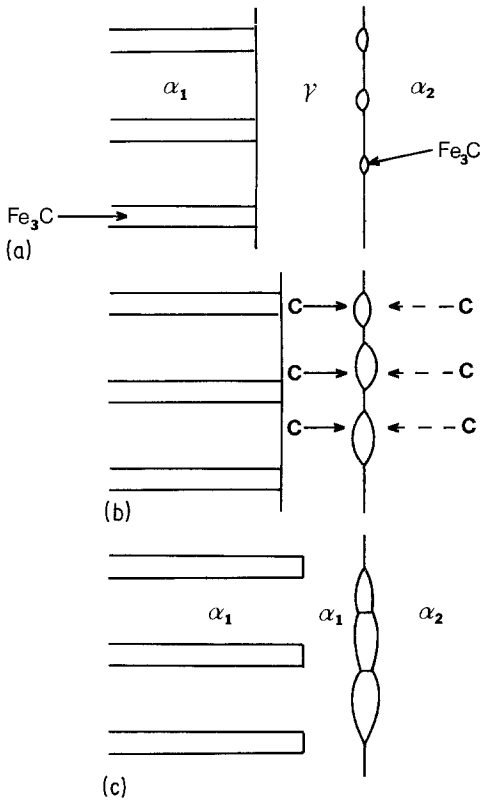

Figure 26 Schematic illustration of the development of massive cementite films at proeutectoid ferrite/pearlite interfaces. (a) Initial stage, (b) intermediate stage, (c) final stage.

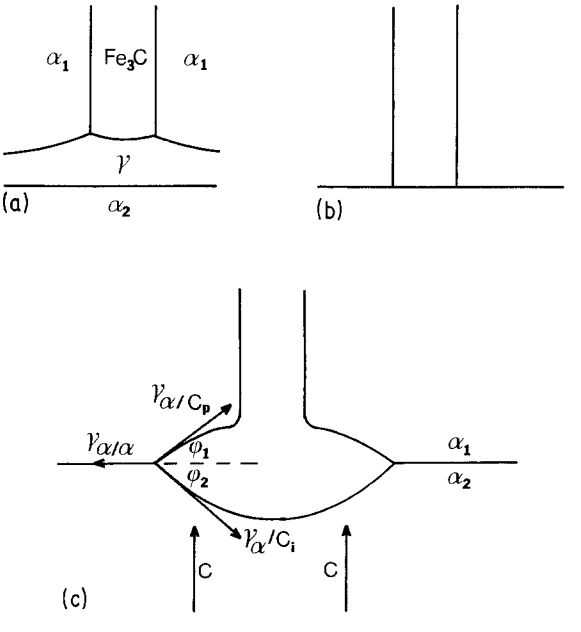

Figure 27 Schematic illustration of the formation of a "club-like" morphology at pearlite/proeutectoid ferrite interfaces, (a) prior to impingement, (b) immediately following impingement, (c) after equilibration.

ferrite/austenite interface prior to impingement with a pearlite colony. (c) Alternatively, the films at proeutectoid ferrite/pearlite interfaces can form by coarsening and coalescence of the pearlitic cementite which is in contact with proeutectoid ferrite/pearlite interfaces.

4. Cementite films of the type noted in points 3a and 3b above, form by multiple nucleation of cementite at proeutectoid ferrite/austenite interfaces.

5. Puckering of the grain boundaries accompanies discrete cementite precipitation.

6. Proeutectoid is the active nucleus for pearlite and the results suggest that pearlite can form by more than one mechanism.

Acknowledgements

The authors wish to thank the American Iron and Steel Institute (A.I.S.I.) for financial support. They are also grateful to Dr G. Ludkovsky of Inland Steel, Chicago for the supply of materials and to Dr S. W. Thompson for many stimulating discussions.

References

1. F. C. HULL and R. F. MEHL, *Trans. ASM* **30** (1942) 381.
2. R. F. MEHL and W. C. HAGEL, in "Progresses in Metal Physics", edited by B. Chalmers and R. King (Pergamon, London, 1956).
3. V. F. ZACKAY and H. I. AARONSON (eds.), "Decompostion of Austenite by Diffusional Process" (Interscience, New York, 1962).
4. M. HILLERT, in *ibid.*, p. 289.
5. S. MODIN, *Jernkont Ann* **135** (1951) 169.
6. M. E. NICHOLSON, *J. Metals* **6** (1954) 1071.
7. R. J. DIPPENAAR and R. W. K. HONEYCOMBE, *Proc. R. Soc. Lond.* **333** (1973) 455.
8. F. H. SAMUELS and A. A. HUSSEIN, *Trans. Iron Steel Inst. Jpn* **23** (1983), 65.
9. H. C. H. CARPENTER and J. M. ROBERTSON, *J. Iron Steel Inst.* **123C** (1934) 345.
10. R. L. RICKETT and F. C. KRISTNFEK, *Trans. ASM* **41** (1949) 1113.
11. N. P. ALLEN, W. P. REES, B. E. HOPKINS and H. R. TIPLER, *J. Iron Steel Inst.* **174** (1953) 108.
12. D. T. GOETTGE and E. L. ROBINSON, *Trans. AIME* **206** (1956) 1169.
13. W. F. CARTWRIGHT and M. F. DOWDING, *J. Iron Steel Inst.* **188** (1958) 23.
14. W. C. LESLIE, R. M. FISHER and N. SEN, *Acta Metall* **7** (1959) 632.
15. A. HULTGREN and H. OHLIN, *Jernkont Ann* **144** (1960) 356.
16. V. E. KAUCZOR, *Arch. Eisenhuttenw.* **35** (1964) 1111.
17. G. OATES, *J. Iron Steel Inst.* **206** (1968) 930.
18. P. N. RICHARDS, *J. Aust. Inst. Met.* **14** (1969) 1.
19. L. E. SAMUELS, "Optical Microscopy of Carbon Steels" (ASM, Metals Park, Ohio, 1980).
20. H. DRAR and H. FISCHMEISTER, *Z. Metallkde* **72** (1981) 821.
21. W. CARRINGTON, K. F. HALE and D. McLEAN, *Proc. R. Soc. A.* **259** (1960) 203.
22. R. A. FOURNELLE and J. B. CLARK, *Metal Trans.* **3** (1972) 2757.
23. S. W. THOMPSON, PhD Thesis, Pennsylvania State University (1986).
24. "Atlas of Isothermal Transformation and Cooling Transformation Diagrams" (ASM, Metals Park, Ohio, 1977).
25. L. G. T. DAVY and S. G. GLOVER, *J. Aust. Inst. Met.* **13** (2) (1968) 71.
26. J. -W. LEE, S. W. THOMPSON and P. R. HOWELL, *J. Mater. Sci.*, to be submitted.
27. A. S. KEH and W. C. LESLIE, *Mater. Sci. Res.* **1** (1963) 208.
28. S. W. THOMPSON, J. -W. LEE and P. R. HOWELL, *Acta Metall.* to be submitted.

Received 10 November 1986
and accepted 28 January 1987